Characterization of free radicals in clathrate hydrates of pyrrole, thiophene and isoxazole by muon spin spectroscopy

Mina Mozafari, Lalangi Chandrasena**,** Iain McKenzie, Kerim Samedov, and Paul W. Percival

M. Mozafari, L. Chandrasena, I. McKenzie, P.W. Percival. Department of Chemistry and TRIUMF, Simon Fraser University, Burnaby, B.C. V5A 1S6, Canada

K. Samedov. Department of Chemistry, University of British Columbia, Vancouver, BC V6T 1Z1, Canada

Corresponding author: Paul Percival (e-mail: percival@sfu.ca)

manuscript submitted for consideration for the SFU Special Issue

Characterization of free radicals in clathrate hydrates of pyrrole, thiophene and isoxazole by muon spin spectroscopy

Mina Mozafari, Lalangi Chandrasena**,** Iain McKenzie, Kerim Samedov, and Paul W. Percival

Abstract

Gas hydrates have long been of interest to the petrochemical industry but there has been growing interest in potential applications for carbon dioxide sequestration and hydrogen storage. This has prompted many fundamental studies of structure and host-guest interactions, but there has been relatively little investigation of chemical reactions of the guest molecules. In previous work we have shown that it is possible to use muon spin spectroscopy to characterize H-atom-like muonium and muoniated free radicals formed in clathrate hydrates. Muonium forms in clathrate hydrates of cyclopentane and tetrahydrofuran, whereas furan and its dihydro- derivatives form radicals. The current work extends studies to clathrates hydrates of other 5-membered heterocycles: thiophene, pyrrole and isoxazole. All form structure II hydrates. In addition to the clathrates, pure liquid samples of the heterocycles were studied to aid in the assignment of radical signals and for comparison with the enclathrated radicals. Similar to furan, two distinct radicals are formed when muonium reacts with thiophene and pyrrole. However, only one muoniated radical was detected from isoxazole. Muon, proton and nitrogen hyperfine constants were determined and compared with values predicted by DFT calculations to aid the structure assignments. The results show that Mu adds preferentially to the carbon adjacent to the heteroatom in thiophene and pyrrole, and to the carbon adjacent to O in isoxazole. The same radicals are formed in clathrates, but the spectra have broader signals, suggesting slower tumbling. Furthermore, additional signals in the avoided level-crossing spectra indicate anisotropy consistent with restricted motion of the radicals in the clathrate cages.

Key words: gas hydrate, clathrate, free radical, muonium, muon spin spectroscopy

Introduction

Clathrate hydrates are ice-like crystalline materials in which guest molecules are trapped inside cages made of hydrogen-bonded water molecules.[1,2] The term "gas hydrate" is used to denote clathrates which contain small organic guest molecules, such as methane. They occur naturally and have been discovered in deep-sea sediments and in permafrost regions of Canada and Siberia.[3] Although these deposits represent an untapped source of fossil fuel and petrochemicals, estimated to exceed known conventional oil resources,[4] extraction would be difficult and involves significant environmental concerns.[5] Even before mining was contemplated, gas hydrates were recognized as a serious hazard in the oil and gas industry – they can form spontaneously in natural gas pipelines, leading to blockages, pipeline rupture, and potentially to explosions.[6] The explosion hazard is amplified by the rapid increase in volume when a gas hydrate decomposes – methane hydrate can generate about 160 times its own volume of gas at standard temperature and pressure. On the other hand, the large storage capacity of clathrate hydrates has led to suggestions for their use in carbon dioxide sequestration[7] and hydrogen storage.[8] Furthermore, the well-defined cage structure and size-specific intercage diffusion of guest molecules might lead to applications of clathrate hydrates for gas separation[9] and for matrix isolation of reactive species, even to their use as "nano-reactors".[10]

The crystal lattice structures of clathrate hydrates are determined by the size of their guest molecules.[1,2] Structures I and II are cubic and contain two sizes of cavity: dodecahedrons (5^{12}) and tetradecahedrons ($5^{12}6^2$) in the case of Structure I; and dodecahedrons (5^{12}) and the larger hexadecahedrons ($5^{12}6^4$) for Structure II. Structure H is hexagonal and has two smaller cages (5^{12} and $4^3 5^6 6^3$) and a much larger cavity ($5^{12}6^8$). The stability of these structures depends on temperature, pressure and the nature of the guest molecules. It is not necessary for all the cages to be filled, so the compositions are generally non-stoichiometric. In some cases (always for type H) a "helper" gas (e.g. nitrogen or xenon) occupies small cages and promotes the stability of clathrates containing much larger molecules in the big cavities. With few exceptions (the so-called semi-clathrates),[11] there is no formal chemical bond between the guest molecule and the host, although there may be hydrogen bonding.[12] Thus, depending on the strength of the

host-guest interaction and their relative sizes, there may be tumbling or more restricted rattling of the guest within its cage.

Most fundamental research on gas hydrates concerns their structure, formation and inhibition, with relatively few studies to date on chemical reactions. The transport of guest molecules through the lattice, and their potential for reaction are clearly relevant to applications that involve storage (particularly of hydrogen) and this has motivated several computational investigations.[13-15] On the experimental side, the standard tools used for clathrate characterization (X-ray and neutron diffraction, solid-state NMR, and Raman spectroscopy)[16] are not generally suitable for studying guest transport and reactions (although not impossible).[17] A more direct approach is to create isolated reactive species and monitor their behaviour with a specific probe (e.g. ESR for free radicals). Thus, hydrogen atoms have been created and studied in several clathrate systems by gamma radiolysis.[18-20] Similarly, small organic free radicals have been created by radiolysis at low temperature and their behaviour monitored by ESR as the temperature was raised.[21-25] There is clear evidence from some of these experiments of H-atom transfer from an alkyl radical in one cavity to a guest molecule in a neighbouring cage.[26-28]

Our own experiments make use of muonium as an H-atom analogue. Muonium (Mu = μ^+e^-) is a single-electron atom with a positive muon (mass 0.11343 u) as nucleus, and is effectively a light isotope of hydrogen.[29,30] It can therefore add to an unsaturated molecule to form a free radical. Muonium and muoniated radicals can be studied by means of muon spin spectroscopy,[31-33] which provides similar information (hyperfine constants) as ESR and ENDOR. However, muons are short-lived (τ = 2.197 μs) particles that are generated at high-energy particle accelerators. There are only a few high intensity sources of muons in the world; we make use of the TRIUMF[34] cyclotron, in Vancouver, BC, Canada. An advantage of using a muon beam is that muons can be implanted in any material. Furthermore, beams can be tuned for a high degree of spin polarization, so that relatively few muons (millions) are needed to give a detectable signal. Since muoniated species are studied in isolation there are no complications due to radical-radical reactions.

In previous work we have shown that muonium can be unambiguously detected in clathrate hydrates of cyclopentane and tetrahydrofuran,[35] whereas cyclopentene, 2,5-dihydrofuran, 2,3-dihydrofuran, and furan itself all give rise to muoniated radicals.[35,36] It

is significant that two distinct radical products were identified for each of furan and 2,3-dihydrofuran, corresponding to Mu addition at inequivalent unsaturated carbon atoms. The current work extends studies to clathrates hydrates of other 5-membered heterocycles: thiophene, pyrrole and isoxazole. All form structure II hydrates, similar to furan, except that a helper gas was necessary to promote formation of the clathrates of thiophene and pyrrole. In addition to the clathrates, pure liquid samples of the heterocycles were studied to aid in the assignment of radical signals and for comparison with the enclathrated radicals.

Experimental

Thiophene, pyrrole and isoxazole were obtained from Sigma-Aldrich and subjected to several freeze-pump-thaw cycles to remove dissolved gases. Neat liquid samples were sealed in stainless-steel cells with steel foil windows for muon irradiation. A polycrystalline sample of isoxazole clathrate hydrate was prepared under oxygen-free conditions, in the same manner as previously describe for furan.[36] A modified procedure was used to make the double hydrates of thiophene-xenon and pyrrole-methane. A mixture of crushed ice and the organic liquid (5.88 mole %) was loaded into a precooled pressure vessel, purged with argon gas, and then pressurized with xenon or methane as appropriate. The pressure cell was kept in dry ice for a few days and subsequently in a freezer at -30 °C until the pressure dropped, consistent with hydrate formation. Powder X-ray diffraction and magic-angle-spinning solid-state NMR (^{129}Xe NMR for the thiophene-xenon hydrate and ^{13}C NMR for the pyrrole-methane hydrate) were used to characterize the samples.

Muon spin spectroscopy experiments were carried out at TRIUMF, using spin-polarized positive muons from the M15 and M20 beam lines. Two types of spectrum were acquired: transverse-field muon spin precession (TF-μSR) and avoided level-crossing resonance (μLCR). Both used the same sample and spectrometer (HELIOS), but with a slightly different arrangement of scintillator detectors. In addition, the spin polarization of the muon beam was oriented parallel to the HELIOS magnetic field for μLCR, and transverse for TF-μSR. Further details can be found in earlier publications.[32,36-38]

Of relevance here is that TF-μSR can reveal the muon spin precession frequencies of muoniated radicals. At high magnetic field each radical gives a pair of precession frequencies separated by the isotropic muon hyperfine constant, A_μ:[39]

(1) $\nu_{R1} = \nu_m - \frac{1}{2} A_\mu$

(2) $\nu_{R2} = \nu_m + \frac{1}{2} A_\mu$

where the mid-point

(3) $$\nu_m = \frac{1}{2}\left[\sqrt{A_\mu^2 + (\nu_e + \nu_\mu)^2} - \nu_e + \nu_\mu \right]$$

is shifted from the muon Larmor frequency ν_μ by a small amount that depends on the relative magnitudes of the muon hyperfine constant A_μ and the electron Larmor frequency ν_e. The frequencies are conveniently displayed in a Fourier power spectrum, but pertinent quantitative parameters (frequencies, amplitudes, relaxation times) are obtained by fitting the original time series.

The other technique, μLCR, provides access to the hyperfine constants (hfcs) of other spin-active nuclei in the radical. The magnetic field is swept and each nucleus gives rise to a resonance at the specific field where there is muon spin depolarization caused by mixing of spin states:

(4) $$B_{\Delta M=0} = \frac{1}{2}\left[\frac{(A_\mu - A_k)}{(\gamma_\mu - \gamma_p)} - \frac{(A_\mu + A_k)}{\gamma_e} \right]$$

where γ_μ, γ_p, γ_e are the muon, proton and electron gyromagnetic ratios, respectively, and A_k is the hyperfine constant to be determined. A second type of μLCR occurs if there is some off-diagonal coupling of spin states, as can happen with the anisotropic part of the hyperfine interaction. In this case the resonance field depends only on the muon hfc:

(5) $$B_{\Delta M=1} = \frac{1}{2} A_\mu \left[\frac{1}{\gamma_\mu} - \frac{1}{\gamma_e} \right].$$

Optimized geometries and hfcs of muoniated free radicals were calculated using DFT methods as implemented in Gaussian09 software.[40] Muonium was treated as a light isotope of H with mass 0.113429 u and magnetic moment 8.890597 μ_N. Vibrational isotope effects were also taken into account, as described previously.[35,36]

Results and Discussion

Identification of Radical Products

Prior to discussing the free radical chemistry of the clathrates studied, it is useful to inspect the results obtained with the neat liquid samples. Not only are the radical signals stronger in this medium, but there should be better correspondence between the hfcs determined in the liquid phase and those predicted by DFT calculations on isolated molecules. Also, there seems to be only limited information in the literature on the protiated equivalents (H atom adducts of thiophene, pyrrole and isoxazole).[41-44]

In previous work we showed that two distinct radicals are formed when muonium reacts with furan.[36] Similar behaviour might well be expected for Mu addition to thiophene and pyrrole (Scheme 1) and this is indeed indicated by the TF-μSR spectra (Fig. 1). Since these are Fourier power spectra, the relative signal amplitudes correspond to the squares of the yields. Evidently Mu addition to the two sites in pyrrole is more specific than for thiophene (which is similar to furan). The situation is even more marked for isoxazole, where only one radical was detected (Fig. 2), although in principle there could be as many as four radical products (Scheme 2). The radical signal intensity is also weaker for isoxazole than for pyrrole and thiophene. However, this does not necessarily imply a smaller radical yield. This is because the signal intensity also depends on the rate of formation of the radical (signal intensity is reduced due to loss of phase coherence caused by different spin precession frequencies in Mu and the radical).[45] Hydrogen abstraction by Mu is generally slow and would not be competitive with addition to a double bond. Accordingly we attribute the weaker radical signals for isoxazole to a slower reaction.

Scheme 1. Muonium addition to furan, thiophene and pyrrole. Hydrogen atoms are only shown for those locations where there is significant hyperfine interaction with the unpaired electron.

Figure 1. Fourier power TF-μSR spectra obtained from liquid samples of (a) thiophene and (b) pyrrole at -9 °C and 11.6 kG. The truncated signal at the muon Larmor frequency (157 MHz) is due to muons in diamagnetic environments. The intense signals at (a) -11.9

MHz and 327.8 MHz and (b) -59.3 MHz and 376.1 MHz correspond to radicals with muon hfcs 339.8 MHz and 435.4 MHz, respectively. The less abundant radicals give rise to visible precession signals at (a) -83.9 MHz and 401.8 MHz (muon hfc 485.7 MHz); and (b) -122.1 MHz (muon hfc 563.1 MHz).

Scheme 2. Potential routes for muonium addition to isoxazole.

Figure 2. Fourier power TF-μSR spectrum from liquid isoxazole at -9 °C and 11.6 kG. The peaks either side of the diamagnetic signal correspond to a single radical with muon hfc 442.1 MHz.

By analogy with the muoniated radicals formed from furan[31,36] we can confidently assign the stronger signals obtained from thiophene and pyrrole to structures **4** and **6**. It is significant that these radicals have smaller muon hfcs than the other two (**3** and **5**), consistent with the extended unpaired spin distribution in the allylic moieties of **4** and **6**. They are also the more stable radical products, according to our DFT calculations (UB3LYP/6-311G(d,p)): **4** is less energetic than **3** by 51 kJ mol^{-1} and **6** is less energetic than **5** by 38 kJ mol^{-1}. Given the relatively large energy differences, we conclude that the relative yields are a result of kinetic control (differing activation energies) rather than thermodynamic.[36] The assignment of the radical signal obtained from isoxazole is not so straightforward. The DFT calculations indicate that **7** is the most stable radical structure, but for unequivocal assignment we turn to the results of the μLCR investigation. As shown in Fig. 3, four resonance signals were detected, consistent with expectations for the hyperfine interactions of three protons and one nitrogen nucleus with the unpaired electron in radical **7**. Taking into account the muon hfc determined from the TF-μSR experiment, the LCR resonant fields translate (via eq. 4) to the proton and nitrogen hfcs listed in Table 1. Comparison with the computational predictions leads to the assignments shown. There is excellent agreement between the experimental and computed hfcs for the β-CHMu group and the C(4)H proton, but the nitrogen and C(3)H values are less satisfactory. We note that ESR studies have shown that OH·, $SO_4{\cdot}^-$ and $PO_4{\cdot}^{2-}$ all add to the C(5) site of isoxazole, and that the nitrogen couplings are all close to 26 MHz.[46,47]

Since our nitrogen hfc is similar, we assume that our computed value is inaccurate, perhaps due to out-of-plane vibrations.

Figure 3. Segments of the μLCR spectrum obtained from liquid isoxazole at -9 °C

Table 1. Analysis of the μLCR spectrum obtained from liquid isoxazole at -9 °C and comparison of the determined hyperfine constants (in MHz) with those calculated for radical **7**.

Figure 4. Segments of the μLCR spectrum obtained from liquid thiophene at 1 °C.

Figure 5. Segments of the μLCR spectrum obtained from liquid pyrrole at -10 °C.

In principle there is ambiguity in the assignment of the μLCR signals to the radicals formed in thiophene (Fig. 4) and pyrrole (Fig. 5) because translation of each resonance field to a nuclear hfc (eq. 4) requires knowledge of the muon hfc, of which there are two values, corresponding to the two possible muoniated radicals. In practice, the different signal intensities and expected proton hfcs leaves little doubt. Thus, the β-proton hfc in a CHMu group is related to the known muon hfc by the ratio of their magnetic moments (0.301) and additional zero-point vibrational isotope effects.[35] The computational predictions provide further guidance and lead to the assignments shown in Tables 2 and 3. There is good agreement between the experimental and computed hfcs for radicals **3** and **4** (derived from thiophene), and for most of those for **5** and **6** (derived from pyrrole). However, there is considerable doubt about the weak signal at 22.35 kG, which might be due to either the C(4)H or the NH of radical **6**, although the experimental hfc matches neither prediction. On the other hand, the NH proton hfc seems to be very sensitive to basis set, and a calculation with the EPR-II basis set predicts 17.0 MHz, in reasonable agreement with the experimental value of 18.4 MHz.

Table 2. Analysis of the μLCR spectrum obtained from liquid thiophene at 1 °C and comparison of experimental hyperfine constants (in MHz) with those calculated for radical **3** and **4**.

Table 3. Analysis of the μLCR spectrum obtained from liquid pyrrole at -10 °C and comparison of experimental hyperfine constants (in MHz) with those calculated for radical **5** and **6**.

The assignment of the major signals to **4** and **6** is consistent with the limited literature on radiolysis of thiophene and pyrrole.[41-43] The 2-hydrothienyl radical was identified by ESR in an irradiated sample of thiophene adsorbed on silica gel.[43] At room temperature the largest proton hfcs (91 MHz, 38 MHz and 33 MHz) are close to our values for **4**. Similarly, irradiation of pyrrole in adamantane yielded the 2-hydropyrrolyl radical, with proton hfcs (107.6 MHz, 31.7 MHz and 31.1 MHz)[41] which closely match our largest values for **6**. The next value, 12.8 MHz, was attributed to NH and is intermediate between our experimental and calculated values. There seems to be no relevant literature data on H atom addition to C(3) of thiophene or pyrrole. However, OH· was found to add to thiophene in aqueous solution to form 2-hydroxythienyl and 3-hydroxythienyl in the proportion 4:1.[44] The α-proton hfc of the latter was reported to be (-)47.3 MHz, in good agreement with our C(2)H value for radical **3** and consistent with greater localization of the unpaired spin than occurs for 2-hydroxythienyl and radical **4**. OH· addition to pyrrole in aqueous solutions is thought to lead to 2-hydroxypyrrolyl, but no ESR spectrum was reported, due to further reaction.[46] On the other hand, N-methylpyrrole leads to a longer-lived radical whose ESR spectrum is consistent with the allylic structure of the N-methyl-2-hydroxypyrrolyl radical: there are proton hfcs of (-)33.1 MHz, (-)32.1, and (+)3.0 MHz.[46] These correspond to C(3)H, C(5)H and C(4)H in our muoniated radical **6**. The small value for the C(4)H again suggests that the μLCR resonance at 22.35 kG is due to NH rather than C(4)H.

Interestingly, our results show that the relative sizes of the C(3)H and C(5)H proton hfcs change in the series **2**, **4** and **6**. The relevant carbon atoms are the ends of an allyl π-system, so the proton hfcs should be proportional to the unpaired spin density on those carbons. Thus we deduce that the unpaired spin density on C(5) is less than that of C(3) for radicals **2** and **6**, but the opposite is true for **4**. This would be consistent with partial extension of the allyl π-system to O and N, but not to S.

Radicals in Hydrates

Turning now to the clathrate samples, it is clear from the similarity of the TF-μSR spectra (Figs. 6 and 7) and μLCR spectra (Figs. 8, 9 and 10) to their equivalents obtained from liquid samples that the same radicals are formed. We note that the intensity of the

radical signals in the TF-μSR spectrum is somewhat lower than that in the neat liquid. This may not seem surprising, in view of the lower concentrations of the guest molecules. However, it is not appropriate to apply the concepts of homogeneous kinetics to reactions in a porous medium. Since there is at most one reactive guest molecule in each large ($5^{12}6^4$) cavity, one might suppose that the yield of muoniated radicals is determined by the probability that a muon will stop in a suitably occupied cage. However that view neglects the possibility that the muon stops elsewhere, forms muonium, which then diffuses into the cage occupied by the reactive guest. The variation in TF-μSR signal intensities suggests that kinetics does indeed play a role, as discussed above for the case of isoxazole. Whereas TF-μSR signals can be reduced due to loss of muon spin phase coherence during reaction, μLCR does not suffer this problem. It is therefore significant that the strongest resonances (typically those due to β-CHMu) have similar intensities in liquid and clathrate, indicating that the radical yields are similar in the two phases.

Figure 6. Fourier power TF-μSR spectra obtained from samples of (a) thiophene-xenon hydrate at -30 °C and 10.6 kG, and (b) pyrrole-methane hydrate at -73 °C and 11.5 kG. The peak at -143 MHz in (a) is an artefact caused by reflection of the diamagnetic signal.
Figure 7. Fourier power TF-μSR spectrum from isoxazole hydrate at -13 °C and 11.6 kG. The peak at -62.7 MHz corresponds to a radical with muon hfc 442.5(3) MHz. Its partner at 380 MHz is lost in the noise.
Figure 8. Segments of the μLCR spectrum obtained from isoxazole hydrate at -13 °C
Figure 9. Segments of the μLCR spectrum obtained from thiophene-xenon hydrate at -30 °C
Figure 10. Segments of the μLCR spectrum obtained from pyrrole-methane hydrate at -73 °C

Another notable difference between the TF-μSR spectra in the two phases is the width of the radical signals – they are broader in the hydrates, indicating faster decay of the precession signals. Since muoniated radicals are detected one molecule at a time by TF-μSR, there is no possibility of combination reactions, nor are there other reactive species on the microsecond time-scale. Accordingly, we attribute the faster decay to spin

relaxation consistent with slower tumbling in the clathrate than the liquid. The μLCR spectra also show broader signals for the enclathrated radicals, and this is again attributed to slower tumbling.

The results of our analysis of the μLCR spectra displayed in Figs. 8-10 are summarized in Tables 4-6. There are small changes in hfcs, but the most noticeable difference between the spectra of radicals in the clathrate and liquid phases is the existence of $\Delta M = 1$ signals in the former. These resonances are easily identified and assigned, as they appear at fields determined by the muon hfc alone (eq. 5), and this is already known from the TF-μSR results. As pointed out in our earlier papers, such signals only appear when there is significant anisotropy, consistent with restricted motion of the radicals in the clathrate cages.[35,36] In general, organic clathrate hydrates are stabilized by van der Waals interactions between the guest and the host molecules, and stronger hydrogen bonds are possible where guests have permanent dipoles.[12,49] Even if only transient, hydrogen bonding would provide a "tether" to restrict the motion of guest molecules and the related radical products. The oxygen atom of furan acts as a proton acceptor for H-bonding, whereas the pyrrole NH can act as donor to an oxygen atom in the water framework. Hydrogen bonding is not expected for thiophene, but judging by the intensity of the $\Delta M = 1$ signal observed for radical **4**, there does seem to be some interaction that restricts motion, at least for the radical. In contrast, radical **7** has a relatively weaker signal, suggesting that isoxazole does not bind so strongly to the lattice.

The timescale of the host-guest interaction is another factor that should be considered. Athough molecular dynamics simulations suggest that individual hydrogen bonds have short lifetimes, on the order of picoseconds,[12] the anisotropy revealed by muon spin spectroscopy implies a time-scale of at least microseconds. A possible explanation is that the Bjerrum defects induced in the water structure migrate over a limited region (e.g. water molecules on a hexagonal face of the cage)[17] such that successive hydrogen bonds prevent completely free reorientation of the guest.

Table 4. Analysis of the μLCR spectrum obtained from isoxazole hydrate at -13 °C and assignment of the hyperfine constants to radical **7**.

Table 5. Analysis of the μLCR spectrum obtained from thiophene-xenon hydrate at -30 °C.

Table 6. Analysis of the μLCR spectrum obtained from pyrrole-methane hydrate at -73 °C.

It is interesting to consider the relative yields of radicals for the pairs **4**/**3**, and **6**/**5**, since this is an indication of the relative reactivity of carbons 2 and 3 in thiophene and pyrrole. We determined the relevant ratios from the amplitudes of the CHMu proton resonances in the μLCR spectra and cross-checked them against the intensities of TF-μSR signals. The results indicate that the selectivity is greater for pyrrole than thiophene, but there is no significant different between the phases: 4.7 ± 0.5 and 4.4 ± 0.4 for pyrrole liquid and clathrate; 2.1 ± 0.2 and 2.5 ± 0.2 for thiophene.

Summary

Muon spin spectroscopy has been used to detect and characterize free radicals formed by muonium addition to thiophene, pyrrole and isoxazole in the liquid phase and also as isolated guest molecules in structure II clathrate hydrates. Two distinct radicals were detected in thiophene and pyrrole but only one for isoxazole. Muon, proton and nitrogen hyperfine constants were determined and compared with values predicted by DFT calculations to aid the structure assignments. The results show that Mu adds preferentially to the carbon adjacent to the heteroatom in thiophene and pyrrole, and to the carbon adjacent to O in isoxazole. These findings agree with the limited literature on H and OH· addition to these molecules. The same radicals were identified in clathrates, but the spectra have broader signals, which is attributed to spin relaxation due to slower tumbling. Additional signals in the avoided level-crossing spectra indicate anisotropy consistent with restricted motion of the radicals in the clathrate cages. Mu addition is more specific for pyrrole than thiophene, but enclathration does not appear to change the relative reactivity of the relevant carbon sites.

Acknowledgements

We thank Dr. Jean-Claude Brodovitch and Myles Scollon for assistance with the muon experiments, and the staff of the Centre for Molecular and Materials Science at TRIUMF for technical support. We are grateful to Dr. John Ripmeester for helpful advice on the NMR characterization of clathrates, and Dr. Andrew Lewis for guidance with the NMR

data acquisition. This research was financially supported by the Natural Sciences and Engineering Research Council of Canada and Simon Fraser University. TRIUMF is operated by a consortium of Canadian universities, and receives federal funding via a contribution agreement with the National Research Council of Canada. Some of the muon studies made use of a beam line funded by the Canada Foundation for Innovation (CFI) and the Province of British Columbia. Computing resources were provided by WestGrid and Compute/Calcul Canada.

References

1 Sloan Jr., E. D.; Koh, C. A. *Clathrate Hydrates of Natural Gases*, 3rd ed.; CRC press: Boca Raton, FL, 2008.

2 Koh, C. A., Towards a fundamental understanding of natural gas hydrates. *Chem. Soc. Rev.* **2002,** *31*, 157-167.

3 Koh, C. A.; Sum, A. K.; Sloan, E. D. Gas hydrates: Unlocking the Energy from Icy Cages. *J. Appl. Phys.* **2009**, *106*, 061101.

4 Chong, Z. R.; Yang, S. H. B.; Babu, P.; Linga, P.; Li, X.-S., Review of natural gas hydrates as an energy resource: Prospects and challenges. *Appl. Energy* **2016,** *162* (C), 1633-1652.

5 Kvenvolden, K. A., Potential effects of gas hydrate on human welfare. *Proc. Natl. Acad. Sci. USA* **1999,** *96*, 3420-3426.

6 Englezos, P., Clathrate Hydrates. *Ind. Eng. Chem. Res.* **1993,** *32*, 1251-1274.

7 Babu, P.; Linga, P.; Kumar, R.; Englezos, P., A review of the hydrate based gas separation (HBGS) process for carbon dioxide pre-combustion capture. *Energy* **2015,** *85*, 261-279.

8 Veluswamy, H. P.; Kumar, R.; Linga, P., Hydrogen storage in clathrate hydrates: Current state of the art and future directions. *Appl. Energy* **2014,** *122*, 112-132.

9 Eslamimanesh, A.; Mohammadi, A. H.; Richon, D.; Naidoo, P.; Ramjugernath, D., Application of gas hydrate formation in separation processes: A review of experimental studies. *J. Chem. Thermodyn.* **2012,** *46*, 62-71.

10 Koh, D.-Y.; Kang, H.; Lee, H. Reactive Radical Cation Transfer in the Cages of Icy Clathrate Hydrates. *Korean J. Chem. Eng.* **2015**, *32*, 350-353.

11 Jeffrey, G. A., Water Structure in Organic Hydrates. *Acc. Chem. Res.* **1969,** *2*, 344-352.

12 Alavi, S.; Udachin, K.; Ripmeester, J. A., Effect of Guest-Host Hydrogen Bonding on the Structures and Properties of Clathrate Hydrates. *Chem.-Eur. J.* **2010,** *16*, 1017-1025.

13 Alavi, S.; Ripmeester, J. A., Hydrogen-gas migration through clathrate hydrate cages. *Angew. Chem., Int. Ed*. **2007,** *46*, 6102-6105.

14 Burnham, C. J.; English, N. J., Free-Energy Calculations of the Intercage Hopping Barriers of Hydrogen Molecules in Clathrate Hydrates. *J. Phys. Chem. C* **2016,** *120*, 16561-16567.

15 Vidal-Vidal, A.; Perez-Rodriguez, M.; Pineiro, M. M., Direct transition mechanism for molecular diffusion in gas hydrates. *RSC Adv.* **2016,** *6*, 1966-1972.

16 Rauh, F.; Mizaikoff, B., Spectroscopic methods in gas hydrate research. *Anal. Bioanal. Chem.* **2012,** *402*, 163-173.

17 Moudrakovski, I. L.; Udachin, K. A.; Alavi, S.; Ratcliffe, C. I.; Ripmeester, J. A., Facilitating guest transport in clathrate hydrates by tuning guest-host interactions. *J. Chem. Phys.* **2015,** *142*, 074705.

18 Yeon, S. H.; Seol, J.; Park, Y.; Koh, D. Y.; Kang, Y. S.; Lee, H., Spectroscopic observation of atomic hydrogen radicals entrapped in icy hydrogen hydrate. *J. Am. Chem. Soc.* **2008,** *130*, 9208-9209.

19 Shin, K.; Cha, M.; Kim, H.; Jung, Y.; Kang, Y. S.; Lee, H., Direct observation of atomic hydrogen generated from the water framework of clathrate hydrates. *Chem. Commun.* **2011,** *47*, 674-676.

20 Koh, D. Y.; Kang, H.; Park, J.; Shin, W.; Lee, H., Atomic Hydrogen Production from Semi-clathrate Hydrates. *J. Am. Chem. Soc.* **2012,** *134*, 5560-5562.
21 Bednarek, J.; Lund, A.; Schlick, S., Unstable intermediates in X-irradiated clathrate hydrates: ESR and ENDOR of tetramethylammonium hydroxide pentahydrate (TMNOH). *J. Phys. Chem.* **1996,** *100*, 3910-3916.
22 Takeya, K.; Nango, K.; Sugahara, T.; Ohgaki, K.; Tani, A., Activation Energy of Methyl Radical Decay in Methane Hydrate. *J. Phys. Chem. B* **2005,** *109*, 21086-21088.
23 Takeya, K.; Sugahara, T.; Ohgaki, K.; Tani, A., Electron spin resonance study on gamma-ray-induced radical species in ethylene hydrate. *Radiat. Meas.* **2007,** *42*, 1301-1306.
24 Oshima, M.; Tani, A.; Sugahara, T.; Kitano, K.; Ohgaki, K., Reactions of HOCO radicals through hydrogen-atom hopping utilizing clathrate hydrates as an observational matrix. *Phys. Chem. Chem. Phys.* **2014,** *16*, 3792-3797.
25 Oshima, M.; Kitamura, K.; Tani, A.; Sugahara, T.; Ohgaki, K. Synergistic Formation of Carboxyl and Methyl Radicals in CO_2 + Methane Mixed Gas Hydrates. *J. Phys. Chem. B* **2014**, *118*, 13435-13439.
26 Ohgaki, K.; Nakatsuji, K.; Takeya, K.; Tani, A.; Sugahara, T., Hydrogen transfer from guest molecule to radical in adjacent hydrate-cages. *Phys. Chem. Chem. Phys.* **2008,** *10*, 80-82.
27 Kobayashi, N.; Minami, T.; Tani, A.; Nakagoshi, M.; Sugahara, T.; Takeya, K.; Ohgaki, K., Intermolecular Hydrogen Transfer in Isobutane Hydrate. *Energies* **2012,** *5*, 1705-1712.
28 Sugahara, T.; Kobayashi, Y.; Tani, A.; Inoue, T.; Ohgaki, K. Intermolecular Hydrogen Transfer between Guest Species in Small and Large Cages of Methane + Propane Mixed Gas Hydrates. *J. Phys. Chem. A* **2012**, *116*, 2405-2408.
29 Roduner, E. *The Positive Muon as a Probe in Free Radical Chemistry*; Lecture Notes in Chemistry No. 49; Springer-Verlag: Berlin, 1988; pp 1-8.
30 Rhodes, C. J. Muonium–the Second Radioisotope of Hydrogen–and its Contribution to Free Radical Chemistry. *J. Chem. Soc., Perkin Trans. 2* **2002**, 1379-1396.
31 Percival, P. W.; Kiefl, R. F.; Kreitzman, S. R.; Garner, D. M.; Cox, S. F. J.; Luke, G. M.; Brewer, J. H.; Nishiyama, K.; Venkateswaran, K. Muon Level-Crossing Spectroscopy of Organic Free Radicals. *Chem. Phys. Lett.* **1987**, *133*, 465-470.
32 West, R.; Percival, P. W. Organosilicon Compounds Meet Subatomic Physics: Muon Spin Resonance. *Dalton Transactions* **2010**, *39*, 9209-9216.
33 McKenzie, I. The Positive Muon and μSR Spectroscopy: Powerful Tools for Investigating the Structure and Dynamics of Free Radicals and Spin Probes in Complex Systems. *Annu. Rep. Prog. Chem., Sect. C: Phys. Chem.* **2013**, *109*, 65-112.
34 The acronym TRIUMF stands for Tri-University-Meson Facility, so named for the three founding universities: Simon Fraser University, University of British Columbia, and University of Victoria. Nowadays TRIUMF is operated by a pan-Canadian consortium of 12 full and 7 associate member universities.
35 Percival, P. W.; Mozafari, M.; Brodovitch, J. C.; Chandrasena, L., Organic Free Radicals in Clathrate Hydrates Investigated by Muon Spin Spectroscopy. *J. Phys. Chem. A* **2014,** *118*, 1162-1167.

36 Mozafari, M.; Brodovitch, J. C.; Chandrasena, L.; Percival, P. W., Characterization of Free Radicals in Clathrate Hydrates of Furan, 2,3-Dihydrofuran, and 2,5-Dihydrofuran by Muon Spin Spectroscopy. *J. Phys. Chem. A* **2016,** *120*, 8521-8528.
37 Percival, P. W.; Addison-Jones, B.; Brodovitch, J. C.; Ghandi, K.; Schüth, J., Free radicals formed by H(Mu) addition to pyrene. *Can. J. Chem.* **1999,** *77*, 326-331.
38 Brodovitch, J. C.; Addison-Jones, B.; Ghandi, K.; McKenzie, I.; Percival, P. W.; Schüth, J., Free radicals formed by H(Mu) addition to fluoranthene. *Can. J. Chem.* **2003,** *81*, 1-6.
39 Sometimes, due to weak signals or limited frequency response, only one of the two radical precession signals can be distinguished. However, it is still possible to calculate the muon hyperfine constant from a single radical precession and the diamagnetic frequency. See ref. 38.
40 Frisch, M. J.; Trucks, G. W.; Schlegel, H. B.; Scuseria, G. E.; Robb, M. A.; Cheeseman, J. R.; Scalmani, G.; Barone, V.; Mennucci, B.; Petersson, G. A.; et al. *Gaussian 09, Revisions C.01, D.01, E.01*; Gaussian Inc.: Wallingford, CT, 2013-2016.
41 Lloyd, R. V.; Digregorio, S.; Wood, D. E., EPR study of free-radicals produced in pyrrole by X-irradiation and tritium atom decay. *J. Chem. Phys.* **1978,** *68*, 1813-1816.
42 Saunders, B. B., Reactions of Thiophene with Radiolytically Produced Radicals .2. Solvated Electron and the Hydrogen Atom. *J. Phys. Chem.* **1978,** *82*, 151-154.
43 Nagai, S.; Gillbro, T., Electron spin resonance studies of radicals produced by γ-irradiation of thiophene in the crystalline and adsorbed states. *J. Phys. Chem.* **1979,** *83*, 402-405.
44 Gilbert, B. C.; Norman, R. O. C.; Williams, P. S., Electron spin resonance studies. Part 59. Radical reactions of thiophens: the formation and reactions of some sulphur-conjugated radical-cations. *J. Chem. Soc., Perkin Trans. 2* **1981,** 207-218.
45 Percival, P. W.; Brodovitch, J. C.; Arseneau, D. J.; Senba, M.; Fleming, D. G., Formation of the muoniated ethyl radical in the gas phase. *Physica B* **2003,** *326*, 72-75.
46 Samuni, A.; Neta, P., Electron spin resonance study of the reaction of hydroxyl radicals with pyrrole, imidazole, and related compounds. *J. Phys. Chem.* **1973,** *77*, 1629-1635.
47 Dogan, I.; Steenken, S.; Schulte-Frohlinde, D.; Icli, S., Electron spin resonance and pulse radiolysis studies on the reaction of OH· and $SO_4{\cdot}^-$ radical with five-membered heterocyclic compounds in aqueous solution. *J. Phys. Chem.* **1990,** *94*, 1887-1894.
48 The negative sign is assumed because ESR splittings are not sensitive to the sign of hyperfine couplings.
49 Lim, D.; Park, S.; Ro, H.; Shin, K.; Lee, H., Effect of Guest-Host Hydrogen Bonding on Thermodynamic Stability of Clathrate Hydrates: Diazine Isomers. *J. Phys. Chem. C* **2015,** *119*, 10218-10226.

Table 1. Analysis of the μLCR spectrum obtained from liquid isoxazole at -9 °C and comparison of the determined hyperfine constants (in MHz) with those calculated for radical **7**.

B_{LCR} (kG)	exptl. hfc	calc. hfc [a]	assignment
	442.1(1)[b]	446.0	β-CH**Mu**
15.667(3)	24.9(1)	16.1	**N**
17.143(4)	121.5(1)	122.3	β-C**H**Mu
22.597(25)	20.5(5)	9.3	C(3)**H**
25.661(11)[c]	-36.3(2)	-34.8	α-C(4)**H**

[a] UB3LYP/6-311G(d,p) with anharmonic vibrational averaging at -9 °C.
[b] Determined by TF-μSR at -9 °C.
[c] Scanned at -10 °C.

Table 2. Analysis of the μLCR spectrum obtained from liquid thiophene at 1 °C and comparison of experimental hyperfine constants (in MHz) with those calculated for radical **3** and **4**.

B_{LCR} (kG)	exptl. hfc	calc. hfc [a]	radical	assignment
	339.76(2)[b]	342.2	**4**	β-CH**Mu**
	485.50(4)[b]	454.8	**3**	β-CH**Mu**
13.216(1)	92.4(1)	93.0	**4**	β-C**H**Mu
19.254(2)	125.2(1)	111.8	**3**	β-C**H**Mu
19.954(2)	-32.5(1)	-32.9	**4**	C(3)**H**
20.141(2)	-35.9(1)	-35.0	**4**	C(5)**H**
28.375(2)	-45.3(1)	-15.6[c]	**3**	α-C(2)**H**

[a] UB3LYP/6-311G(d,p) with anharmonic vibrational averaging at 1 °C.
[b] Determined by TF-μSR at -9 °C.
[c] Unexplained discrepancy. The values are -54.5 MHz for the equilibrium geometry, and -39.4 MHz after vibrational averaging at 0 K.

Table 3. Analysis of the μLCR spectrum obtained from liquid pyrrole at -10 °C and comparison of experimental hyperfine constants (in MHz) with those calculated for radical **5** and **6**.

B_{LCR} (kG)	exptl. hfc	calc. hfc [a]	radical	assignment
	435.4(1)[b]	436.6	**6**	β-CH**Mu**
	563.1(1)[b]	564.3	**5**	β-CH**Mu**
17.495(3)	108.3(1)	111.8	**6**	β-C**H**Mu
22.346(12)[c]	18.4(2)	5.9[d]	**6**	[N**H**][c]
22.346(12)[c]	18.4(2)	8.1	**6**	[C(4)**H**][c]
22.670(12)	139.2(2)	149.6	**5**	β-C**H**Mu
25.041(4)	-31.5(1)	-29.8	**6**	C(5)**H**
25.155(2)	-33.6(1)	-33.6	**6**	C(3)**H**

[a] UB3LYP/6-311G(d,p) with anharmonic vibrational averaging at -10 °C.
[b] Determined by TF-μSR at -9 °C.
[c] Alternative assignments of very weak signal.
[d] 17.0 MHz if calculated with UB3LYP/EPR-II.

Table 4. Analysis of the μLCR spectrum obtained from isoxazole hydrate at -13 °C and assignment of the hyperfine constants to radical **7**.

B_{LCR} (kG)	hfc (MHz)	assignment
15.702(12)	23.7(4)	**N**
16.224(9)[a]	441.9(2)	β-CH**Mu**
17.198(5)	120.3(3)	β-C**H**Mu

[a] $\Delta M = 1$ resonance.

Table 5. Analysis of the μLCR spectrum obtained from thiophene-xenon hydrate at -30 °C.

B_{LCR} (kG)	hfc (MHz)	radical	assignment
12.632(4)[a]	344.1(1)	**4**	β-CH**Mu**
13.451(6)	92.6(3)	**4**	β-C**H**Mu
18.047(5)[a]	491.6(1)	**3**	β-CH**Mu**
19.638(8)	124.4(4)	**3**	β-C**H**Mu
20.201(11)	-32.5(3)	**4**	C(3)**H**
20.343(10)	-35.2(3)	**4**	C(5)**H**

[a] $\Delta M = 1$ resonance.

Table 6. Analysis of the μLCR spectrum obtained from pyrrole-methane hydrate at -73 °C.

B_{LCR} (kG)	hfc (MHz)	radical	assignment
16.384(2)[a]	446.3(1)	**6**	β-CH**Mu**
18.185(3)	106.4(1)	**6**	β-C**H**Mu
20.851(8)[a]	568.0(2)	**5**	β-CH**Mu**
23.028(9)	137.5(2)	**5**	β-C**H**Mu
25.649(8)	-32.0(2)	**6**	C(5)**H**
25.762(10)	-34.0(2)	**6**	C(3)**H**

[a] $\Delta M = 1$ resonance.

Scheme 1. Muonium addition to furan, thiophene and pyrrole. Hydrogen atoms are only shown for those locations where there is significant hyperfine interaction with the unpaired electron.

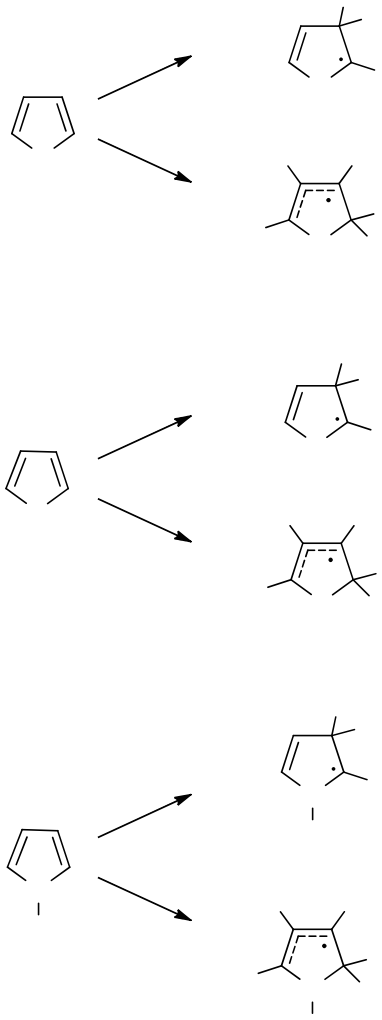

Scheme 2. Potential routes for muonium addition to isoxazole.

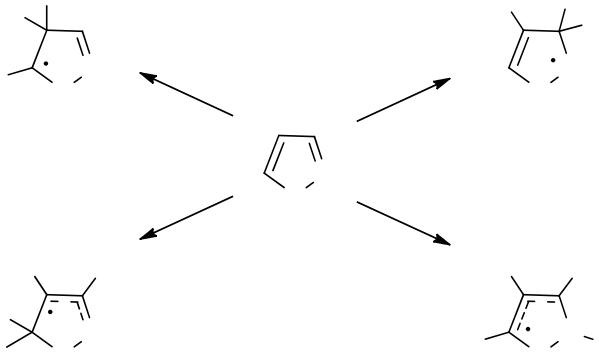

8 Mu

H

H

7

Mu

H_β

Figure 1. Fourier power TF-μSR spectra obtained from liquid samples of (a) thiophene and (b) pyrrole at -9 °C and 11.6 kG. The truncated signal at the muon Larmor frequency (157 MHz) is due to muons in diamagnetic environments. The intense signals at (a) -11.9 MHz and 327.8 MHz and (b) -59.3 MHz and 376.1 MHz correspond to radicals with muon hyperfine constants 339.8 MHz and 435.4 MHz, respectively. The less abundant radicals give rise to visible precession signals at (a) -83.9 MHz and 401.8 MHz (muon hyperfine constant 485.7 MHz); and (b) -122.1 MHz (muon hyperfine constant 563.1 MHz).

Figure 2. Fourier power TF-μSR spectrum from liquid isoxazole at -9 °C and 11.6 kG. The peaks either side of the diamagnetic signal correspond to a single radical with muon hyperfine constant 442.1 MHz.

Figure 3. Segments of the μLCR spectrum obtained from liquid isoxazole at -9 °C.

Figure 4. Segments of the μLCR spectrum obtained from liquid thiophene at 1 °C.

Figure 5. Segments of the μLCR spectrum obtained from liquid pyrrole at -10 °C.

Figure 6. Fourier power TF-μSR spectra obtained from samples of (a) thiophene-xenon hydrate at -30 °C and 10.6 kG, and (b) pyrrole-methane hydrate at -73 °C and 11.5 kG. The peak at -143 MHz in (a) is an artefact caused by reflection of the diamagnetic signal.

Figure 7. Fourier power TF-μSR spectrum from isoxazole hydrate at -13 °C and 11.6 kG. The peak at -62.7 MHz corresponds to a radical with muon hfc 442.5(3) MHz. Its partner at 380 MHz is lost in the noise.

Figure 8. Segments of the μLCR spectrum obtained from isoxazole hydrate at -13 °C

Figure 9. Segments of the μLCR spectrum obtained from thiophene-xenon hydrate at -30 °C

Figure 10. Segments of the μLCR spectrum obtained from pyrrole-methane hydrate at -73 °C

Fig. 1

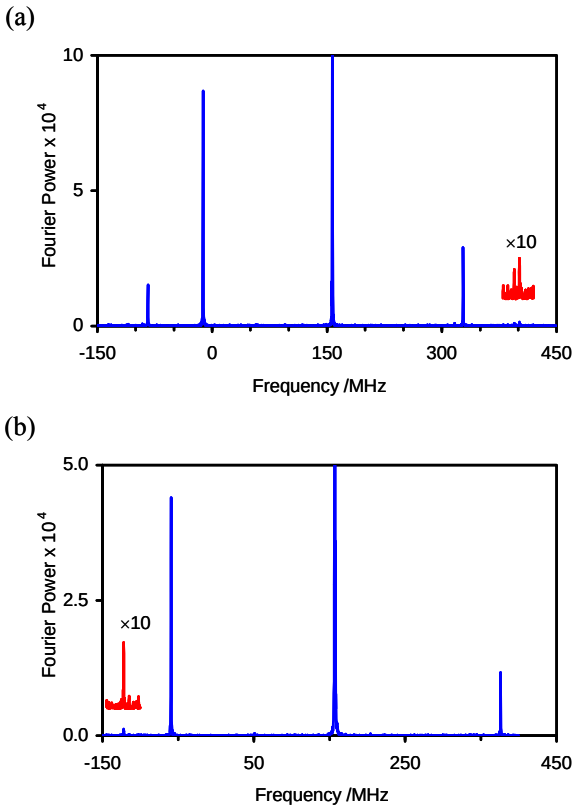
(a)
10
5
0
Fourier Power x 10^4
×10
-150
0
150
300
450
Frequency /MHz
(b)
5.0
2.5
0.0
Fourier Power x 10^4
×10
-150
50
250
450
Frequency /MHz

Fig. 2

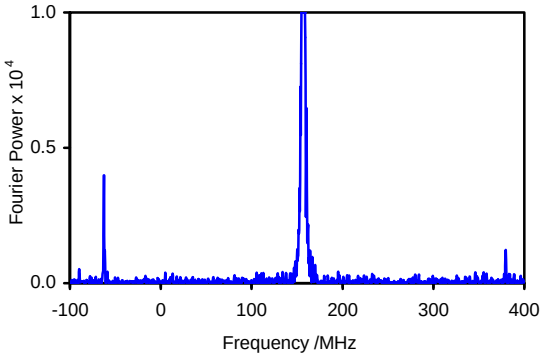
1.0
0.5
0.0
Fourier Power x 10^4
-100
0
100
200
300
400
Frequency /MHz

Fig. 3

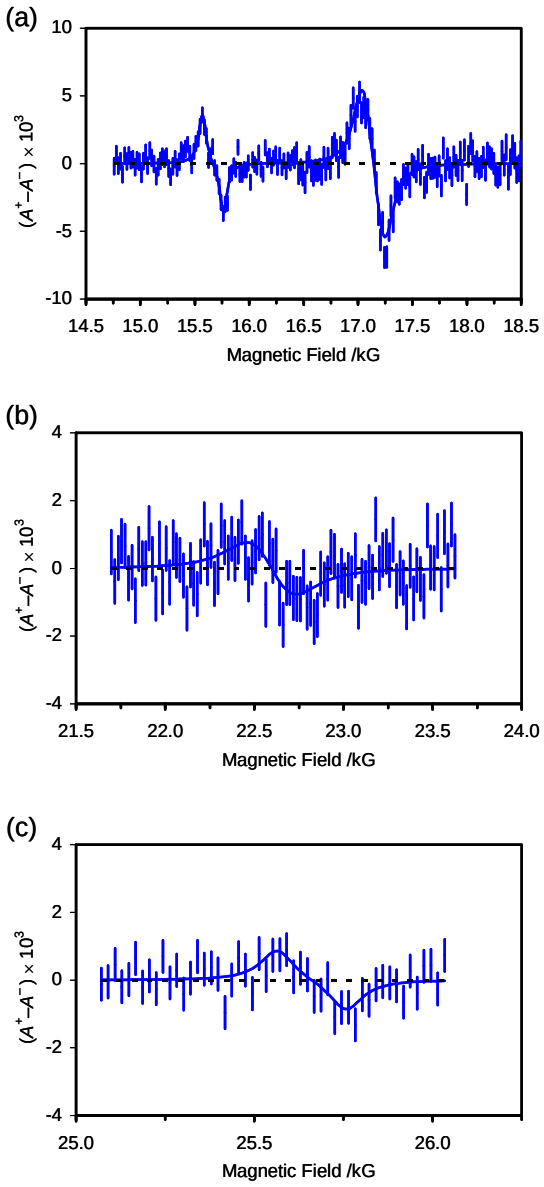
(a)
10
5
0
-5
-10
$(A^+-A^-)\times10^3$
14.5
15.0
15.5
16.0
16.5
17.0
17.5
18.0
18.5
Magnetic Field /kG
(b)
4
2
0
-2
-4
$(A^+-A^-)\times10^3$
21.5
22.0
22.5
23.0
23.5
24.0
Magnetic Field /kG
(c)
4
2
0
-2
-4
$(A^+-A^-)\times10^3$
25.0
25.5
26.0
Magnetic Field /kG

Fig. 4

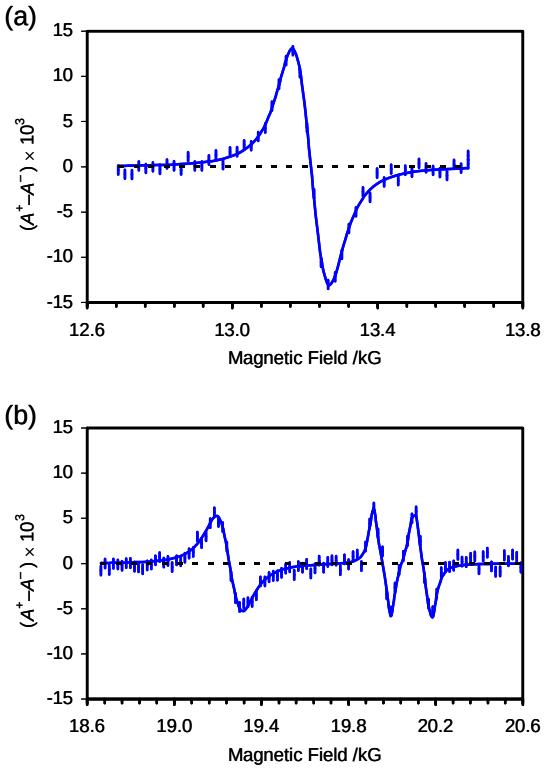
(a)
15
10
5
0
-5
-10
-15
$(A^+ - A^-) \times 10^3$
12.6
13.0
13.4
13.8
Magnetic Field /kG
(b)
15
10
5
0
-5
-10
-15
$(A^+ - A^-) \times 10^3$
18.6
19.0
19.4
19.8
20.2
20.6
Magnetic Field /kG

Fig. 5

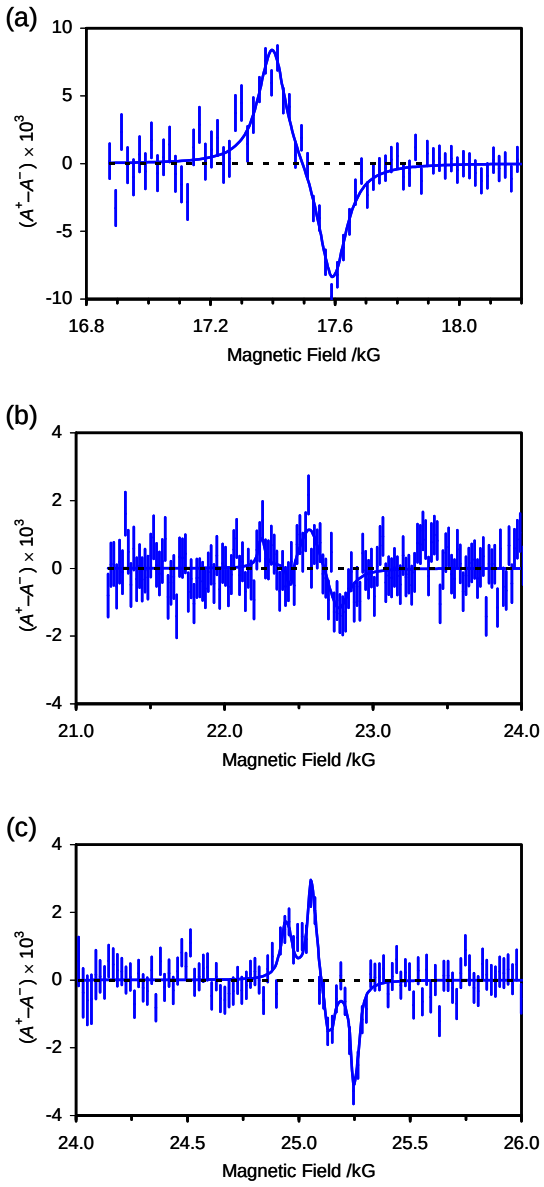
(a)
10
5
0
-5
-10
16.8
17.2
17.6
18.0
Magnetic Field /kG
(A+–A−) × 10³
(b)
4
2
0
-2
-4
21.0
22.0
23.0
24.0
Magnetic Field /kG
(A+–A−) × 10³
(c)
4
2
0
-2
-4
24.0
24.5
25.0
25.5
26.0
Magnetic Field /kG
(A+–A−) × 10³

Fig. 6

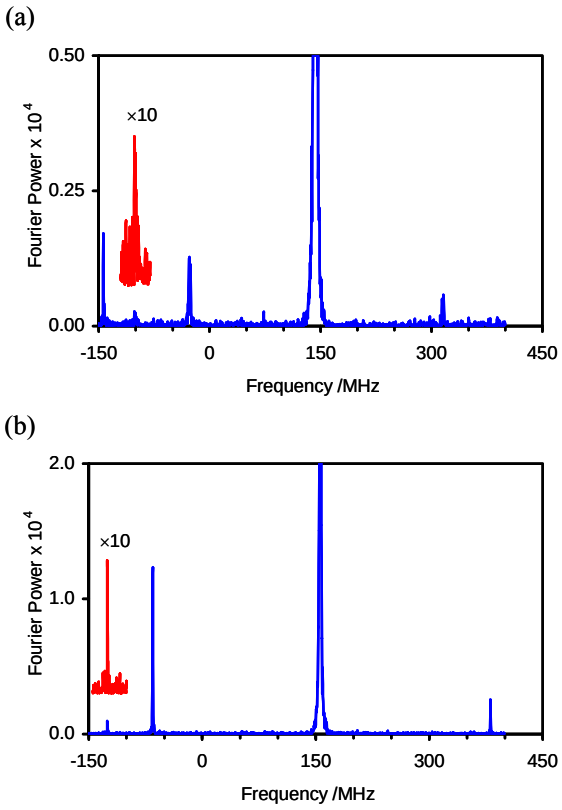
(a)
0.50
0.25
0.00
×10
Fourier Power x 10^4
-150
0
150
300
450
Frequency /MHz
(b)
2.0
1.0
0.0
×10
Fourier Power x 10^4
-150
0
150
300
450
Frequency /MHz

Fig. 7

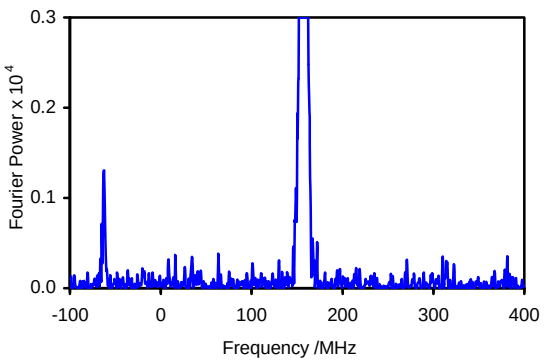
0.3
0.2
0.1
0.0
Fourier Power x 10^4
-100
0
100
200
300
400
Frequency /MHz

Fig. 8

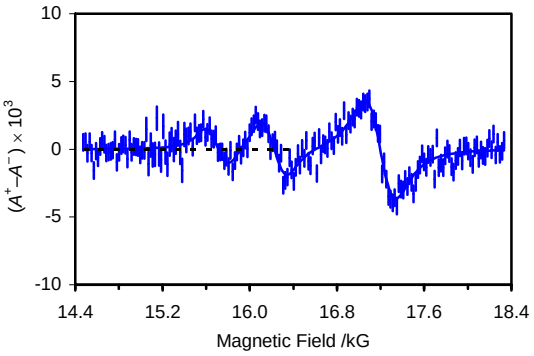
10
5
0
-5
-10
14.4
15.2
16.0
16.8
17.6
18.4
Magnetic Field /kG
$(A^+ - A^-) \times 10^3$

Fig. 9

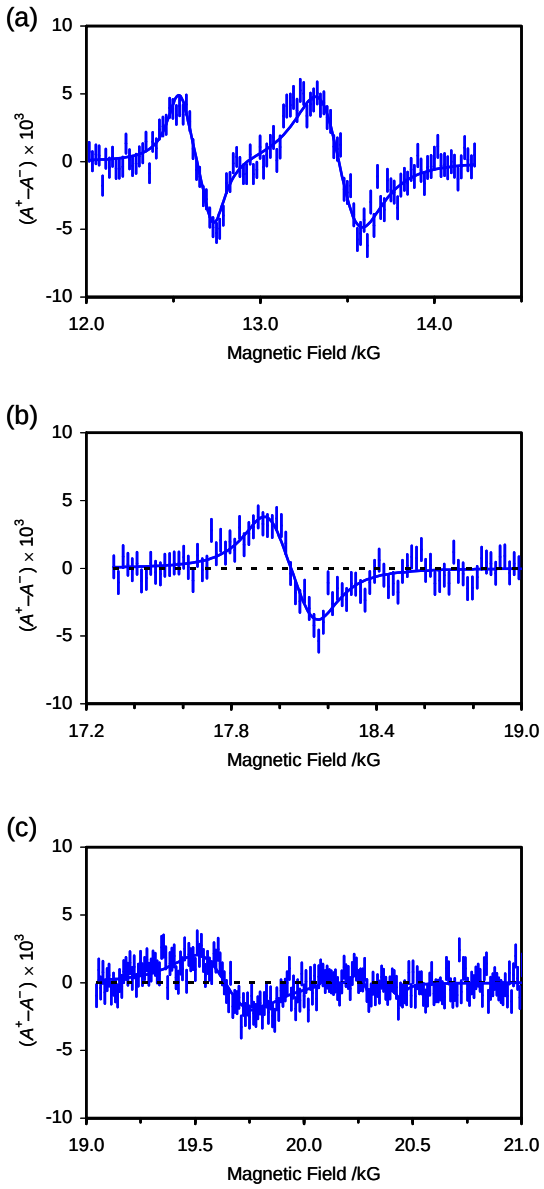
(a)
10
5
0
-5
-10
12.0
13.0
14.0
$(A^+ - A^-) \times 10^3$
Magnetic Field /kG
(b)
10
5
0
-5
-10
17.2
17.8
18.4
19.0
$(A^+ - A^-) \times 10^3$
Magnetic Field /kG
(c)
10
5
0
-5
-10
19.0
19.5
20.0
20.5
21.0
$(A^+ - A^-) \times 10^3$
Magnetic Field /kG

Fig. 10

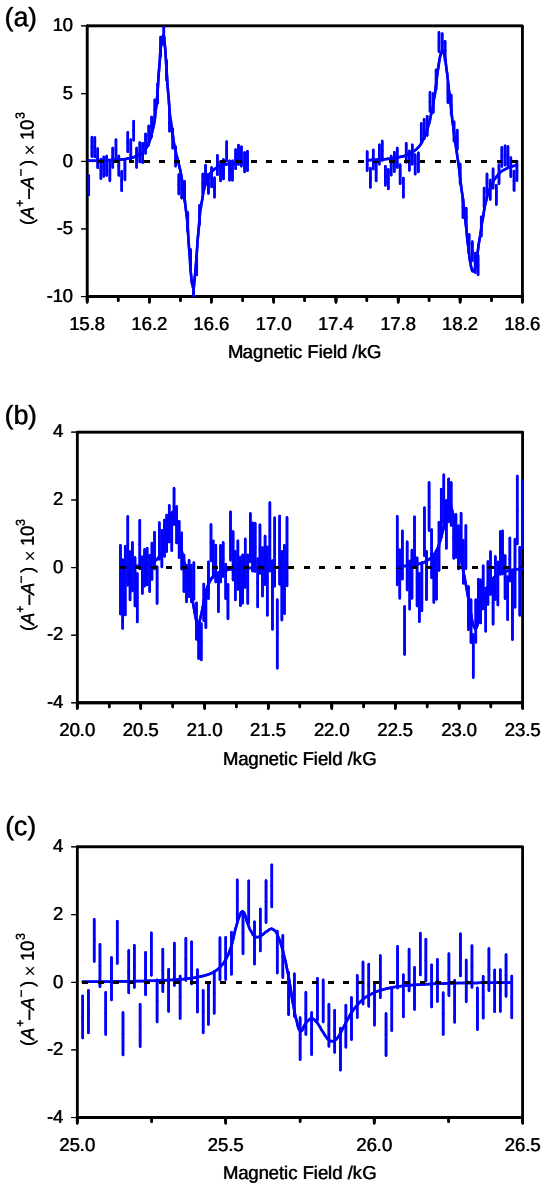
(a)
10
5
0
-5
-10
$(A^+-A^-)\times10^3$
15.8
16.2
16.6
17.0
17.4
17.8
18.2
18.6
Magnetic Field /kG
(b)
4
2
0
-2
-4
$(A^+-A^-)\times10^3$
20.0
20.5
21.0
21.5
22.0
22.5
23.0
23.5
Magnetic Field /kG
(c)
4
2
0
-2
-4
$(A^+-A^-)\times10^3$
25.0
25.5
26.0
26.5
Magnetic Field /kG

TOC graphic